Experimental Study of Evolution of Breach Resulting from Piping at Upper Part of Earth-Fill Dam

Mehmet Şükrü GÜNEY[1]
Merve OKAN[2*]
Emre DUMLU[3]
Aslı BOR[4]
Gökmen TAYFUR[5]
Pelin AKLIK[6]

ABSTRACT

Piping and overtopping are the most important causes of earth-fill dam failure. Such dams may erode under seepage, causing a reduction in the structural strength. The aim of this study was to investigate the temporal evolution of the breach and flow rate from the breach resulting from the piping in earth-fill dams. The experiments were carried out at Hydraulics Laboratory of Civil Engineering Department of İzmir University of Economics. The dam was constructed by using a mixture consisting of 85 % sand and 15 % fine (low plasticity clay). In the first scenario a circular tunnel with a diameter of 2 cm was created along the centreline at 6 cm below the dam crest whereas in the second one it was located at the upper edge. Six cameras at different locations recorded the evolution of the progress of the breach formation. The pump flow rate was measured by magnetic flow meter, and the continuity equation was used to calculate the flow rate values from the breach. The time-varied values of the total breach areas were determined using the Gauss Area formula. The image processing method

---

1 Izmir University of Economics, Department of Civil Engineering, İzmir, Türkiye
  sukru.guney@ieu.edu.tr - https://orcid.org/0000-0003-1441-4784

2 Izmir University of Economics, Department of Civil Engineering, İzmir, Türkiye
  merve.okan@ieu.edu.tr - https://orcid.org/0000-0001-6095-2992

3 The University of Mississippi, National Center for Computational Hydroscience and Engineering, Oxford, USA
  edumlu@go.olemiss.edu - https://orcid.org/0000-0003-4311-3040

4 Norwegian University of Science and Technology Trondheim, Norway
  Izmir University of Economics, Department of Civil Engineering, İzmir, Türkiye
  asli.b.turkben@ntnu.no - https://orcid.org/0000-0002-1679-5130

5 Izmir Institute of Technology, Department of Civil Engineering, İzmir, Türkiye
  gokmentayfur@iyte.edu.tr - https://orcid.org/0000-0001-9712-4031

6 Izmir University of Economics, Department of Civil Engineering, İzmir, Türkiye
  pelin.aklik@ieu.edu.tr - https://orcid.org/0000-0002-0070-2307

* Corresponding author

was also applied in the determination of the breach areas. The time-dependent changes of water depth in the channel were also recorded. The obtained experimental findings are presented and commented, together with the universal dimensionless curves. The failure of the dams occurred mainly because of the head cut erosion developed from downstream to upstream. When breaching started, the orifice flow was converted to open channel flow where breach bottom behaved like a broad crested weir. In the second scenario, the rigid lateral side considerably influenced the flow rate and the development of the breach. The peak flow rate corresponding to the first scenario was found approximately 2.3 times greater than that of the second one. The maximum values of all the breach parameters were reached earlier in the case of the seepage along the centerline. The ratios between the values corresponding to the first and the second scenarios were found as 3.25 and 1.75 for maximum breach areas at downstream and at upstream sides, respectively. These ratios were 2.44 and 1.37 for the average breach widths at downstream and upstream sides, respectively. A very good agreement was found between the area values obtained from Gauss area method and image processing technique, in both scenarios. This fact demonstrated that either of these two approaches can be used to determine the time-dependent breach areas. These experimental findings provide the opportunities for the calibration and validation of the numerical models used in the relevant numerical investigations. This study also offers guidance for the strategies concerning emergency action plans related to the failure of homogeneous earth-fill dams when the piping starts at upper part of the homogeneous earth-fill dams.

1. INTRODUCTION

Piping due to seepage is considered to be one of the main causes of the dam failure. Piping, caused by seepage, stands as a primary contributor to dam failures. Zhong et al. (2021) [1] analyzed more than 3500 historical cases of embankment dam failures; one of the major failure modes is due to piping/seepage accounting for 35% of all. Internal erosion encompasses processes where soil particles are eroded within or beneath the embankment due to seepage, manifesting itself as final mechanism of backward erosion piping [2]. Piping is a process where seepage forces cause the removal of fine particles along a path from the upstream to the downstream face of a structure [3]. As internal erosion progresses, piping can lead to breaching, with the loss of material escalating the risk of collapse in geotechnical structures due to high seepage pressures [4]. Once the piping channel becomes large enough, the outflow through the breach increases, accelerating the failure. A notable example is the Teton Dam failure, where initial piping triggered internal erosion through cracks in the key trench fill, ultimately leading to the dam's complete collapse, resulting in 11 fatalities and extensive property damage [5].

Temporal development of the breach resulting from piping depends on various factors including the porous medium characteristics, the flow parameters, the dams' geometric properties as well as the piping location. Earth-fill dams are more susceptible to internal erosion and piping due to seepage. As internal erosion and piping due to seepage are the main causes of failure in these dams, the control of seepage is extremely important in dam design and construction [6].

Soil composition plays a vital role in the breach initiation time, breach formation time, breach width, breach height, and the peak outflow. These breaching factors present a significant threat to life and property in the downstream of a dam [7].

Dhiman and Patra (2020) [7] investigated the influence of the soil properties on the breaching process by means of small-scale cohesive and non-cohesive embankments. In all experiments, the embankment height was 0.3 m with a crest width of 0.1 m. The mean particle size (d_{50}) of CL soil and sand were 0.018 mm and 0.52 mm, respectively. The average breach width decreased by 67.5% when the proportion of fine particles was increased from 6% to 16%. Zhu et al. (2011) [8] built 5 embankments (1 with pure sand and 4 with various sand-silt-clay mixtures) to investigate breach evolution. They found that cohesive soil embankments eroded slowly and were significantly affected by head cut erosion. Morris et al. (2008) [9] revealed that instead of simplified approaches, more realistic approaches are required about the breach mechanism as well as the breach geometry and flow through the breach.

Zomorodian et al. (2020) [10] constructed homogeneous earthen dams 0.15 m high, 0.35 m wide and created a groove of 1 cm square at 14 cm from the bottom. The test material was a mixture of uniform sand and fine-grained soil. Their results revealed that the initiation and development of the erosion by overtopping depended on the soil compaction level. Sharif et al. (2015) [11] investigated the piping erosion process in an earthen embankment by creating a hole at the bottom of the dam to initiate the piping. The soil mixture used in these experiments consisted of 64% medium sand, 29% silt and 7% clay. They obtained empirical formulas to predict the erosion depth, the area of vertical erosion and the eroded volume. The ratio of the average erosion depth to the average erosion bottom width was found to be close to one. Elkholy et al. (2015) [12] investigated the piping erosion process in an earthen embankment by creating a hole at the bottom of the dam to initiate the piping. Different soil mixtures classified as silty sand were used with constant upstream head. The researchers reported the occurrence of the maximum depth of erosion on the upstream side and the maximum bottom width of erosion on the downstream side.

Annunziato et al. (2024) [13] analyzed the Derna dam break event that occurred in Libya in September 2023. They modelled the dam break, estimated the flood extent, established its timeline, and compared the model results with the available qualitative or quantitative post-event information.

In various numerical studies, the shape of the breach is typically considered trapezoidal. However, the breach shape actually depends on several parameters including the dam geometry, soil properties, hydraulic conditions as well as the seepage location. Numerous experiments with different scenarios are needed to provide accurate data for use in numerical analyses. Since many images in the literature show breaches in their last stages, it is also important to identify and take into account how the geometry of the breach changes with time.

In the literature, there have been many studies on dam failures, particularly those caused by overtopping, but there exist limited piping experiments because of relative difficulties to perform them. This study is a part of the project TUBITAK 119M609, supported financially by the Scientific and Technological Research Council of Turkey. The aim of this project is to investigate the temporal evolution of the breach and flow rate through the breach resulting

from piping starting at different locations of the earth-fill dams. The experiments were carried out at Hydraulics Laboratory of Civil Engineering Department of İzmir University of Economics. The experiments were performed on homogeneous earthen dams, constructed from a mixture of 85 % sand and 15 % fine (low plasticity clay). For the first scenario, a circular tunnel with a diameter of 2 cm was created along the centerline, 6 cm below a homogeneous dam crest whereas in the second one it was located at the upper corner. These scenarios were presented in two different international scientific meetings [14, 15]. The experiments were performed by designing and building dam bodies in laboratory flumes with significant dimensions compared to those available in the literature concerning such experiments performed in the laboratory. The experimental setup, experimental procedures, and soil properties are described in detail. The obtained experimental findings are presented and commented. The objective of this study is to conduct experiments to investigate the development of dam failure resulted from the piping starting at upper part of the earth-fill dams to provide insights into the breach mechanism and data to the relevant researchers who deal with numerical analyses and emergency action plans.

2. EXPERIMENTAL PROCEDURE

The experimental dam was built in a rectangular channel of 1 m wide, 0.81 m high and 5.44 m long, as shown in Fig. 1. The dam having a height of 0.6 m, a bottom width of 2 m and a
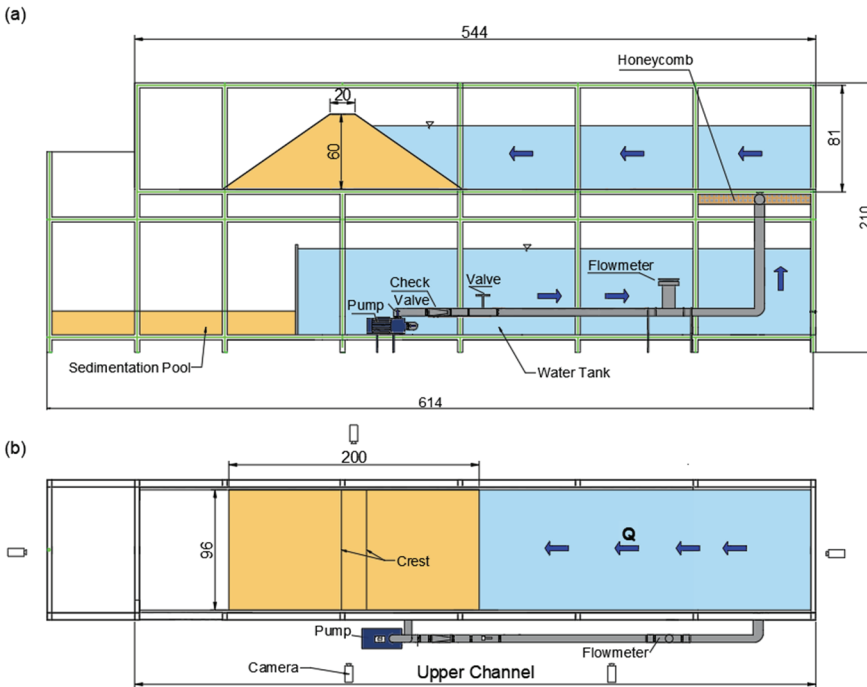

Figure 1 - Experimental system (a) side view, (b) plan view (All dimensions are in cm)

crest width of 0.20 m was built in the upper channel. The slopes of the upstream and downstream sides were set to 1:1.5. Water circulated between the lower reservoir and the upper channel by means of a pump. Soil mechanics tests were carried out in the laboratory before the construction of the dam.

The grain-size distribution curve for soil mixture obtained from sieve analysis (ASTM D-6913) and hydrometer analysis (ASTM D-7928) is given in Fig. 2a. Some characteristic diameter values are as follow; D_{10}=0.006 mm, D_{30}= 0.075 mm, D_{50}= 0.3 mm, and D_{60}= 0.4 mm. The coefficients of uniformity and gradation were found as C_u =66.7 and C_c =2.34, respectively. The soil classified as Clayey Sand with a corresponding symbol SC according to Unified Soil Classification System. The specific gravity for the mixture was found as SG= 2.63 (ASTM D854 – 23).

Proctor test (ASTM D-698) was performed to obtain the maximum dry unit weight and the optimum water content (Fig. 2b). From Fig. 2b, $Y_{dry,max}$= 1.794 gr/cm^3 and w_{opt} = 12.5 %. In the experiments, the energy was reduced by 50 % in order to facilitate the occurrence of piping. The applied compaction energy was 309 kJ/m^3. Hence, the number of blows applied for each layer during the construction of the dam was 13 instead of 25. In the experiments, the bulk density of 1.997 g/cm^3 was satisfied for each layer. Before the compaction, each layer was 14 cm thick and after the compaction it was reduced to 10 cm.

The constant head permeability test (ASTM D-2434) was performed to determine the hydraulic conductivity of the mixture. The coefficient of permeability was obtained as k=0.00047 cm/s. From the Atterberg test (ASTM D-4318), LL was found to be equal to 17.5 %. From the direct shear test (ASTM D-3080) two important parameters for the soil were evaluated as cohesion c= 15.33 kPa and internal friction angle ϕ = 33.93°. According to the consolidation test (ASTM D-2435-04) results, the compression index C_c =0.1, the swell index C_s = 0.007, the recompression index, C_r = 0.009, and E_{oed}= 35714 kPa. The unconfined compression test (ASTM D2166-00) was realized with 3 different loading increments. The unconfined compression index C_{un} value was found as 9.95 kPa.

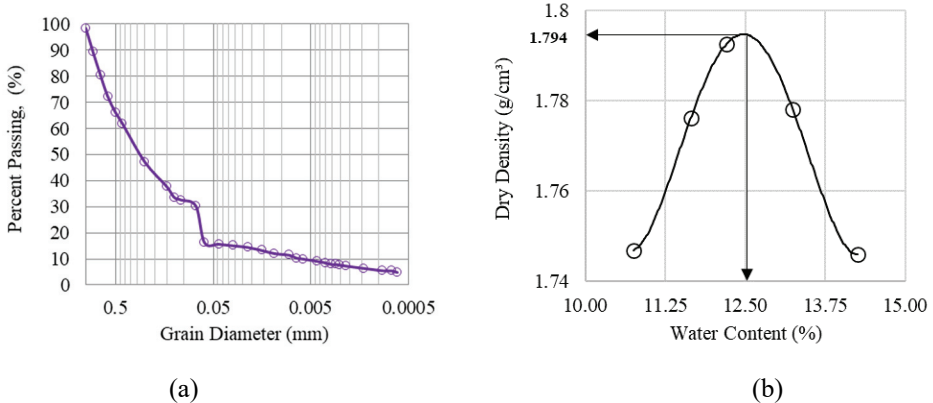(a)   (b)

Figure 2 - a) Grain size distribution of soil mixture with sieve analysis and hydrometer analysis b) dry density versus water content graph

The properties of the mixture used in the dam construction are summarized in Table 1.

Table 1 - Soil mixture Properties

% Fine (Low plasticity clay)	15
% Sand	85
Cohesion, c (kPa)	15.3
Angle of Friction, ϕ (°)	33.9
Specific Gravity, SG	2.63
D_{50} (mm)	0.3
The coefficient of Permeability (cm/s)	0.00047
Liquid Limit, LL (%)	17.5
Optimum Water Content (%) (25 blows)	9.8
Max. Dry Density (g/cm³) (25 blows)	1.886
Optimum Water Content (%) (13 blows)	12.5
Max. Dry Density (g/cm³) (13 blows)	1.794
Oedometric modulus of deformation, E_{oed} (kPa)	35714

The dam was constructed layer by layer. Each layer of 14 cm was compacted so that its thickness becomes 10 cm by using Proctor Hammer and plate. Some construction stages and finished shape of the dam body are given in Fig. 3.

(a) (b) (c) (d)
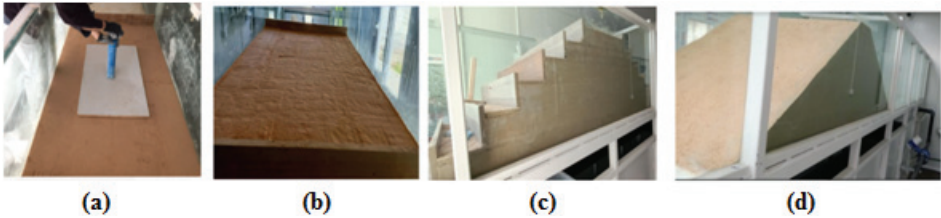
Figure 3 - Some construction stages: (a) Compacting by proctor hammer, (b) After compaction of the first layer, (c) After compaction of the last layer, (d) Final shape
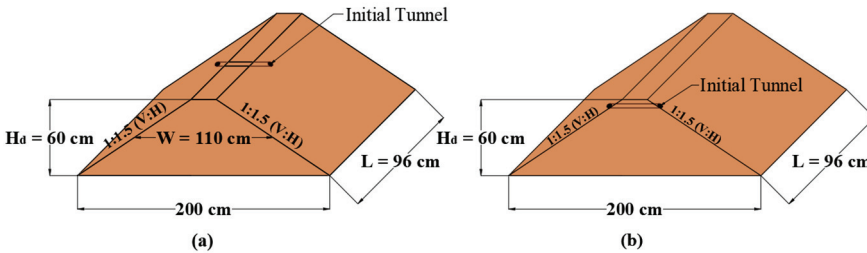

(a) (b)

Figure 4 - Schematic views of the dam body corresponding to seepage a) along centerline b) at corner

In order to generate the formation of the breach, a circular hole of 2 cm diameter lying from upstream to downstream was created at 54 cm from the bottom of the dam body (Fig. 4).

3. EXPERIMENTAL RESULTS

The pump flow rate was measured by a magnetic flowmeter. The evolution of the dam failure was recorded by six cameras placed at different locations. In order to adjust the water level, an electromagnetic sensor was attached which starts and stops the pump when water depths in the channel were 0.540 m and 0.555 m, respectively.

The ratio of the local hydraulic gradient to critical hydraulic gradient determines whether the local particle migrates by seepage forces [16, 17, 18 and 19]. The critical hydraulic gradient, i_{cr}, was calculated by $i_{cr} = \frac{(\gamma_{sat} - \gamma_w).(1-n)}{\gamma_w}$; where n is the porosity, γ_{sat} is the saturated unit weight, and γ_w is the unit weight of water [16]. In this study, by using respectively numerical values of 0.32, 21.2 kN/m³, and 10 kN/m³, it was obtained as $i_{cr} = 0.76$.

3.1. Case 1: Piping at the Upper Part along the Centerline

The temporal developments of the breach recorded by the cameras located at downstream and upstream of the dam are given in Fig. 5 and Fig. 6, respectively. The time t=0 corresponds to the starting of the seepage [15, 19]. As seen in Figures 5 and 6, there was head cut erosion proceeding from downstream to upstream. The breach formation started at downstream side first and progresses backward to upstream side.
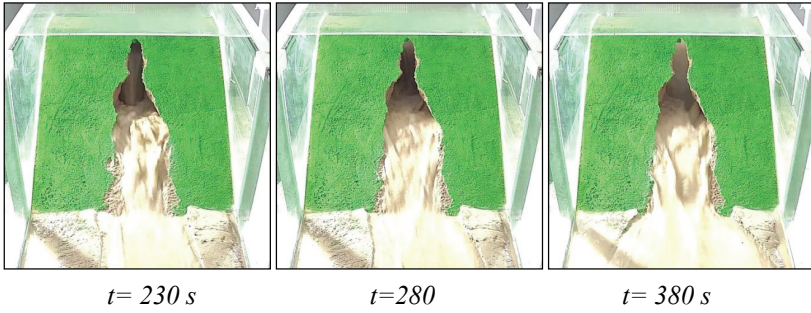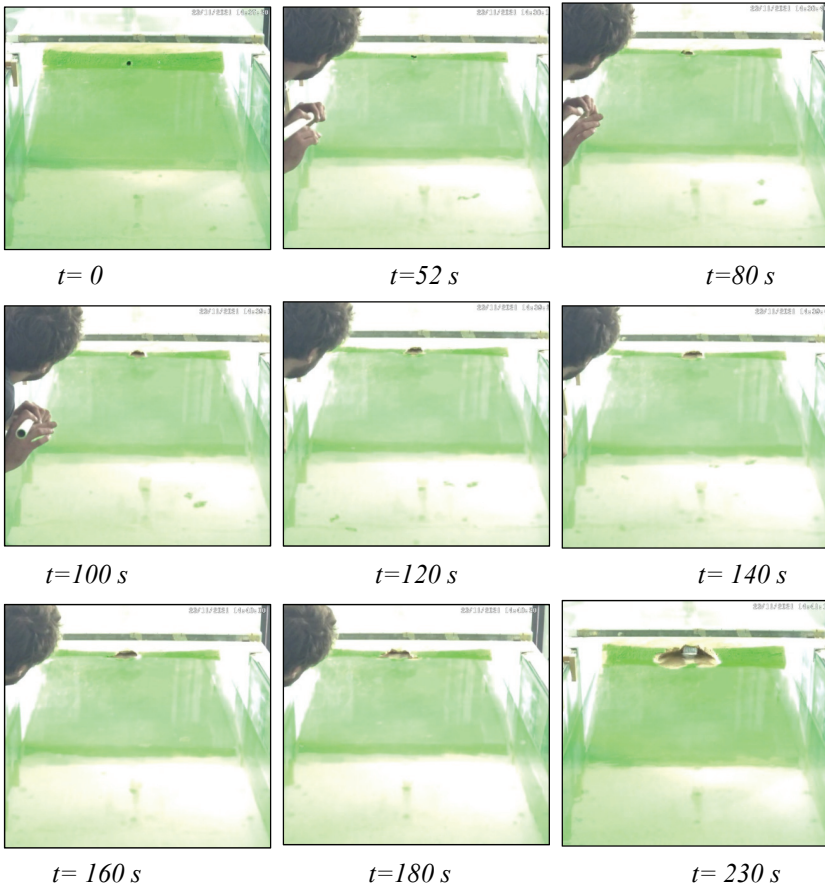

t= 0   t=52 s   t=80 s

t=120 s   t=160 s   t= 180 s

| *t= 230 s* | *t=280* | *t= 380 s* |
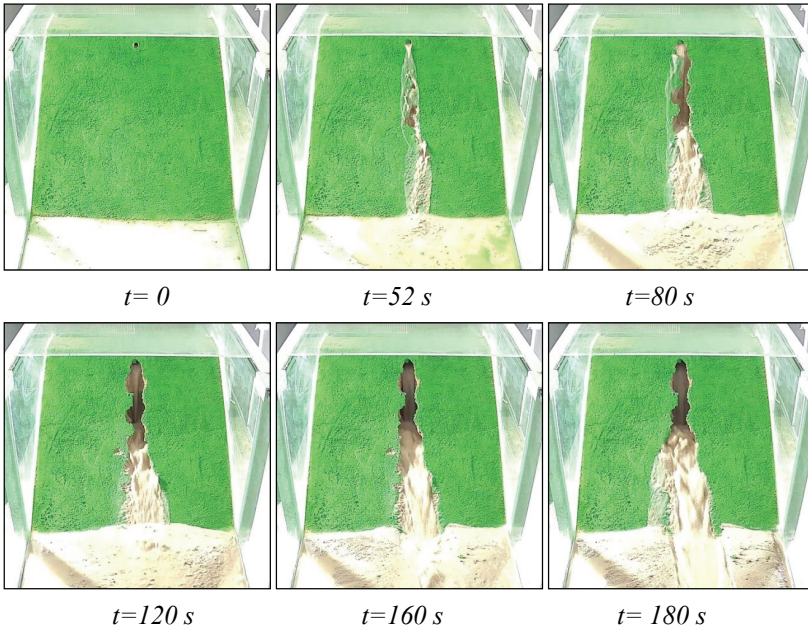
Figure 5 - The temporal development of the central breach at downstream

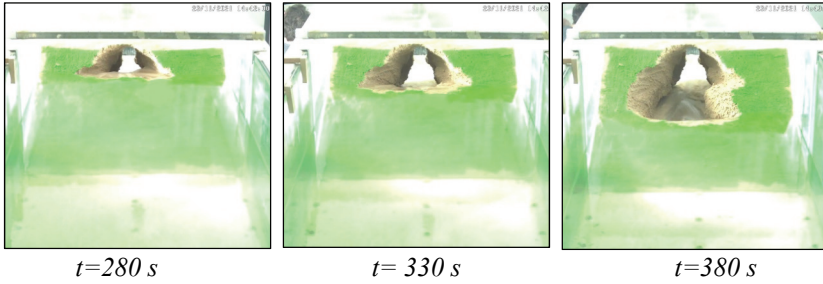| *t= 0* | *t=52 s* | *t=80 s* |
| *t=100 s* | *t=120 s* | *t= 140 s* |
| *t= 160 s* | *t=180 s* | *t= 230 s* |

| t=280 s | t= 330 s | t=380 s |

Figure 6 - The temporal development of the central breach at upstream

The water depths in the channel were obtained from the related camera recordings.

The discharge of water outgoing from the breach was determined by using the continuity equation:

$$\Delta S=(Q_{pump}- Q)\cdot\Delta t \tag{1}$$

where Q_{pump} is the flow rate delivered by the pump, Q is the discharge from the breach, and ΔS is the storage in the channel during the time interval Δt.

The time-varied water level in the upstream reservoir and average discharge from the central breach are given in Fig. 7.
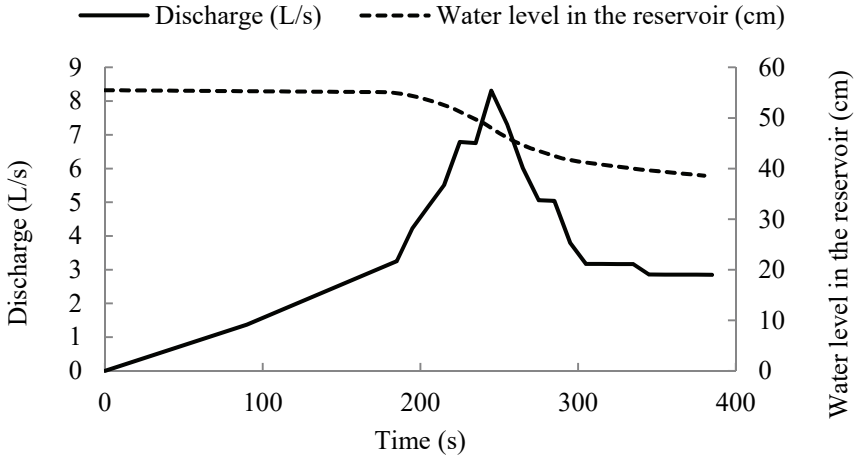
Figure 7 - Time-varied water level in the upstream reservoir and average discharge from the central breach

The maximum discharge from the breach was calculated as Q_{max}=8.31 L/s at t=245 s.

The geometry of the breaches was obtained by examining the images of the cameras located at upstream, downstream and lateral sides. In order not to work with fisheye images, the

videos acquired from lateral camera recordings were edited and straightened using the Hit-film-Express version 2021.1. Besides, extra sensitive solutions were applied to ensure that the images were completely flat. The images obtained from the records corresponding to a certain time were scaled and the boundary coordinates of the breaches were determined in the Get-data Graph Digitizer 2.26 environment.

The time-varied breach areas were calculated by using the Gauss area formula:

$$Area = \frac{1}{2} \sum_{i=1}^{n} x_i(y_{i+1} - y_{i-1}) = \frac{1}{2} \sum_{i=1}^{n} y_i(x_{i+1} - x_{i-1}) \qquad (2)$$

where n is the number of sides, x_i and y_i represent the abscissa and ordinate in the coordinate i, respectively.

The temporal variations of the central breach area at downstream and upstream are presented in Fig. 8.

During the experiment, the breach initiated on the downstream side and then evolved towards to upstream side. As expected, there was a delay in the evolution of the breach at upstream side. At downstream the breach reached its maximum value at t=370 s and remained nearly constant while at upstream side the evolution of the breach continued, and its maximum value was greater than that at downstream.
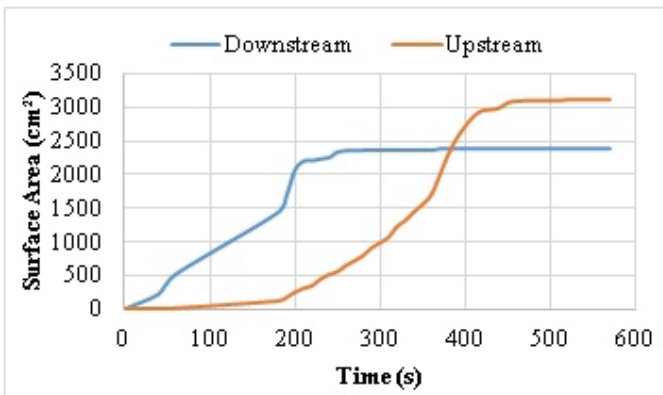

Figure 8 - Temporal variations of the central breach area at downstream and upstream

The maximum breach surface area at the upstream was found to be A_{umax}= 3128.7 cm^2 at t=520 s.

At downstream A_{dmax}= 2379.3 cm^2 at t=370 s and remained unchanged afterwards.

3.2. Case 2: Piping at the Upper Part Corner

This scenario was realized to enable better visualization of the breach development by means of the transparent glass side and the temporal developments of the breach recorded by the

cameras located at downstream, upstream and lateral side of the dam are shown in Figs. 9, 10 and 11, respectively. The time t=0 indicates the beginning of the seepage [14, 19].
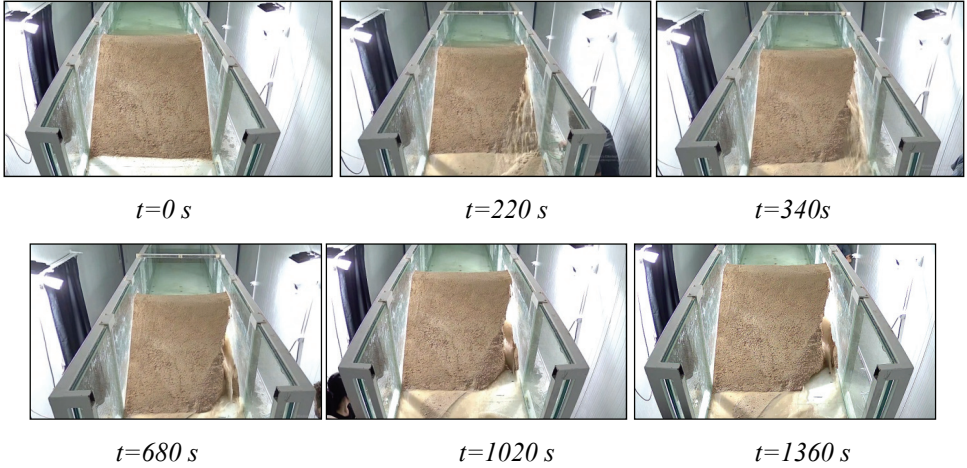

| t=0 s | t=220 s | t=340s |

| t=680 s | t=1020 s | t=1360 s |

Figure 9- The temporal development of the corner breach at downstream

| t=0 s | t=220 s | t=340s | t=680 s |

| t=1020 s | t=1360 s | t=1700s | t=2040 s |
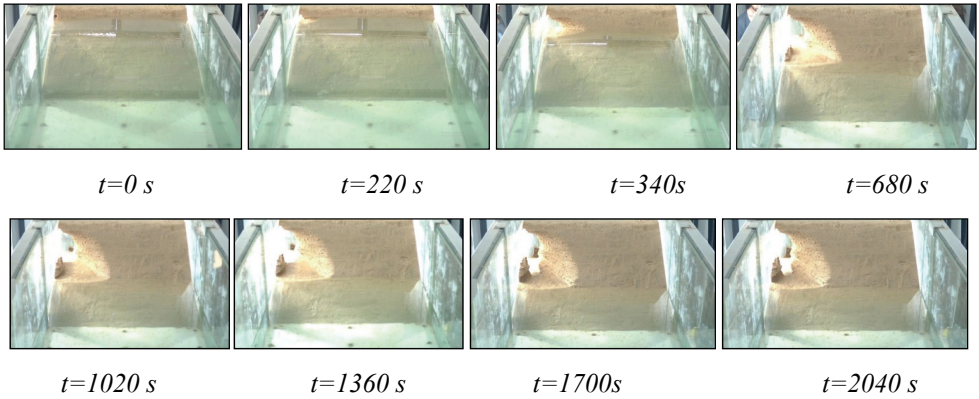
Figure 10 - The temporal development of the corner breach at upstream

| t=0 s | t=220 s | t=340 s |

t=680 s   *t=1020 s*   *t=1360 s*
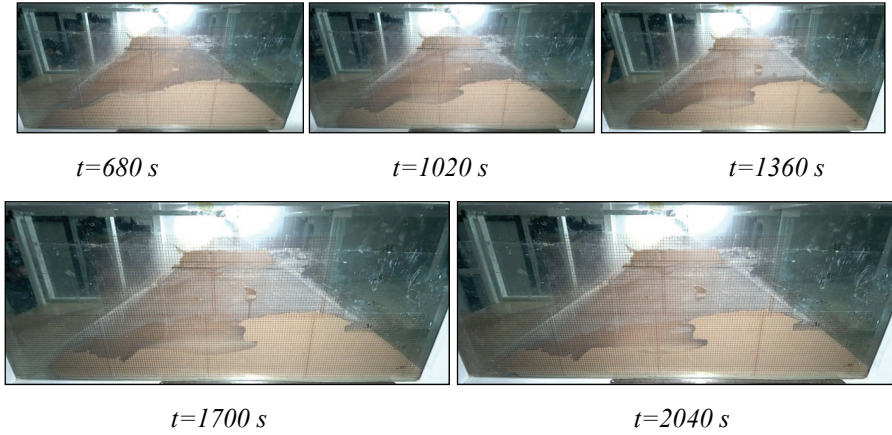
t=1700 s   *t=2040 s*
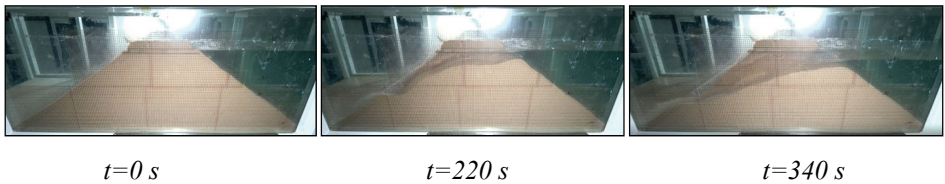
Figure 11 - The temporal development of the corner breach at lateral side

The time-varied water level in the upstream reservoir and average discharge from the corner breach are given in Fig. 12.
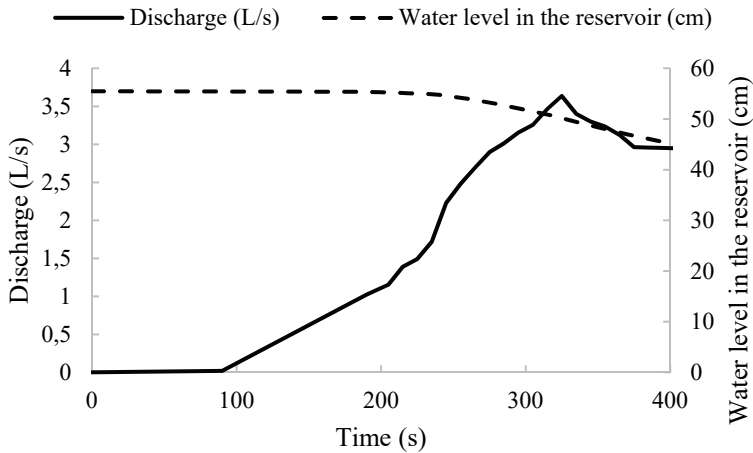

Figure 12 - Time-varied water level in the upstream reservoir and average discharge through the corner breach

The maximum discharge from the breach was calculated as Q_{max}=3.64 L/s at t=320 s. The peak flow rate was found to be quite smaller compared to that found in the 1st scenario (8.31 L/s) and this value was reached later (320 s instead of 245 s.).

The temporal variations of the corner breach area at downstream, upstream and lateral side are presented in Fig. 13.
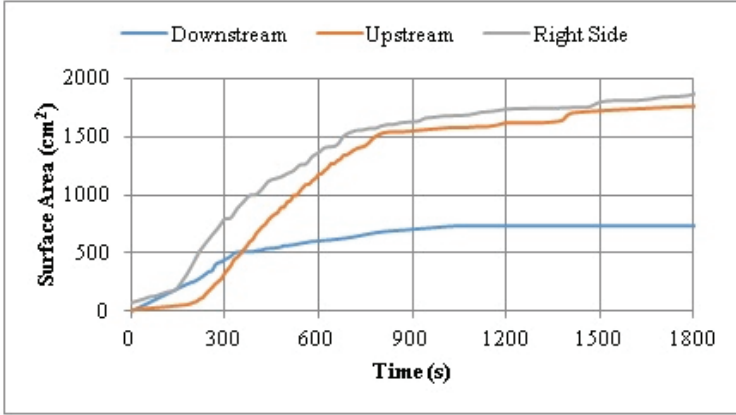
Figure 13 - Temporal variations of the corner breach area at downstream, upstream and lateral side

Some comparative experimental findings are given in Table 2.

The maximum values of all the parameters given in Table 2 were reached earlier in the case of the seepage along the centerline.

Table 2 - Comparison of some experimental parameters

Case (Scenario) number	1	2
Location of the seepage	Upper center	Upper corner
Max. flow rate Q_{max} (L/s)	8.31	3.64
t_Q= time to reach Q_{max} (s)	245	320
Max. breach area at downstream A_{dmax} (cm^2)	2379	733
t_d=time to reach A_{dmax} (s)	370	1080
Max. breach area at upstream A_{umax} (cm^2)	3129	1792
t_u=time to reach A_{umax} (s)	520	1950
Max. avg. breach width at downstream B_{dmax} (cm)	22	9
$t_{B,d}$=time to reach B_{dmax} (s)	370	520
Max. avg. breach width at upstream B_{umax} (cm)	41	30
$t_{B,u}$=time to reach B_{umax} (s)	390	580

Likewise, it was observed that the breach started at the downstream side and then developed towards to upstream side. The delay in the development of the breach at upstream was found to be smaller compared to the 1st scenario. The breach surface area of the upstream was recorded at a maximum level of A_{umax}=1760 cm^2 at t =1800 s. At downstream A_{dmax}= 732 cm^2 at t=1080 s and remained unchanged, also A_{latmax}= 1875 cm^2 at t=1800 s.

4. USE OF IMAGE PROCESSING TECHNIQUE TO ASSESS THE EVOLUTION OF BREACH

The image processing technique was also used to monitor the erosion process for the breach surface area.

Since it was not possible to apply spray paint to the glass side, the surface where erosion occurs was painted with green colour on Matlab environment by using "drawpolygon" command in order to display the eroded area for the case 2.

Matlab Color Thresholder – HSV was used to detect the breach surface areas. The breach areas were obtained by adjusting the HSV colour space. In this study, H, S, and V values were adjusted to detect colours other than green.

Fig.14 illustrates the bottom erosion lines and the average erosion depths corresponding to the 2nd case.
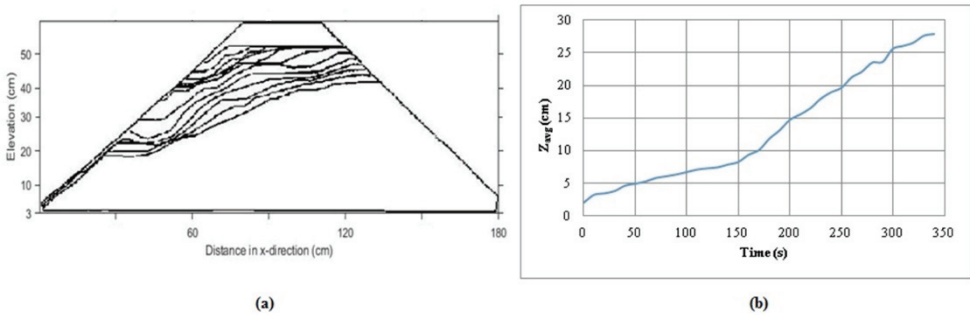

(a)

(b)

Figure 14 - a) Bottom erosion lines for every 30 seconds (starting from t=10 sec) b) Temporal variation of the average erosion depths for case 2

As seen from this figure the average breach depth developed rather slowly in the first half of the experiment period while it developed nearly twice as fast in the second half. Besides, when the first half of the experiment period was completed, the edge of bottom erosion line reached the upstream surface of the dam, and then it was observed that there was an increase in the development of breach depth at the second half of the period.

The time dependent image processing using Matlab Color Thresholder for downstream and upstream sides of the dam corresponding to the 1st case are given in Figs. 15 and 16, respectively.
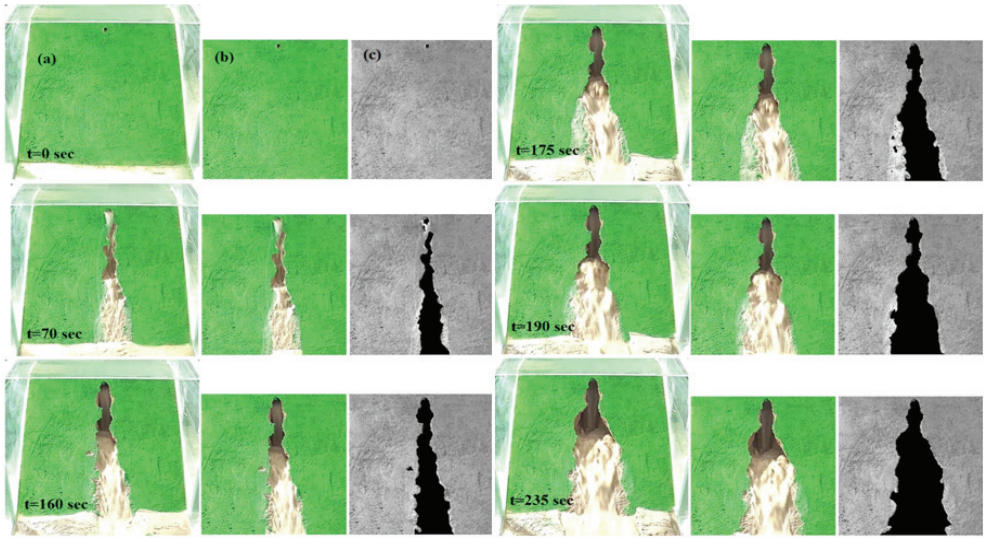
Figure 15 - Time dependent image processing using Matlab Colour Thresholder for downstream – HSV. a) Original picture from experiments. b) Cropped Image c) After Colour Thresholding for case 1
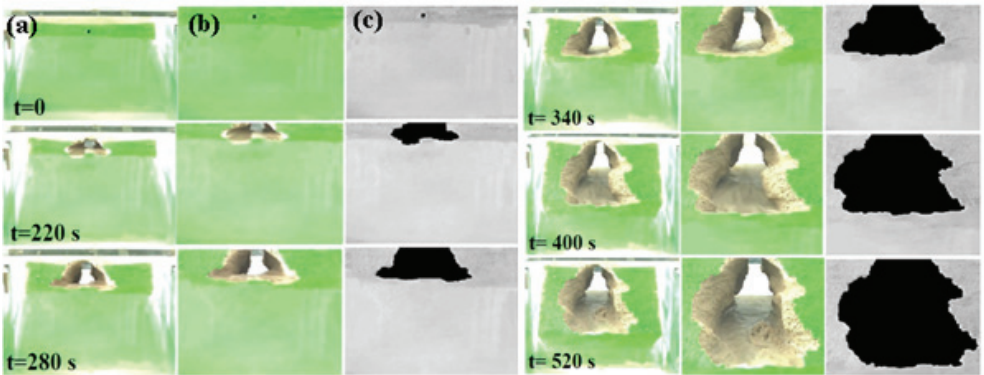

Figure 16. Time dependent image processing using Matlab Colour Thresholder for upstream - HSV. a) Original picture from experiments. b) Cropped Image c) After Colour Thresholding for case 1

Figure 17 represents the evaluation of eroded lateral area at different time instants for the 2nd case.
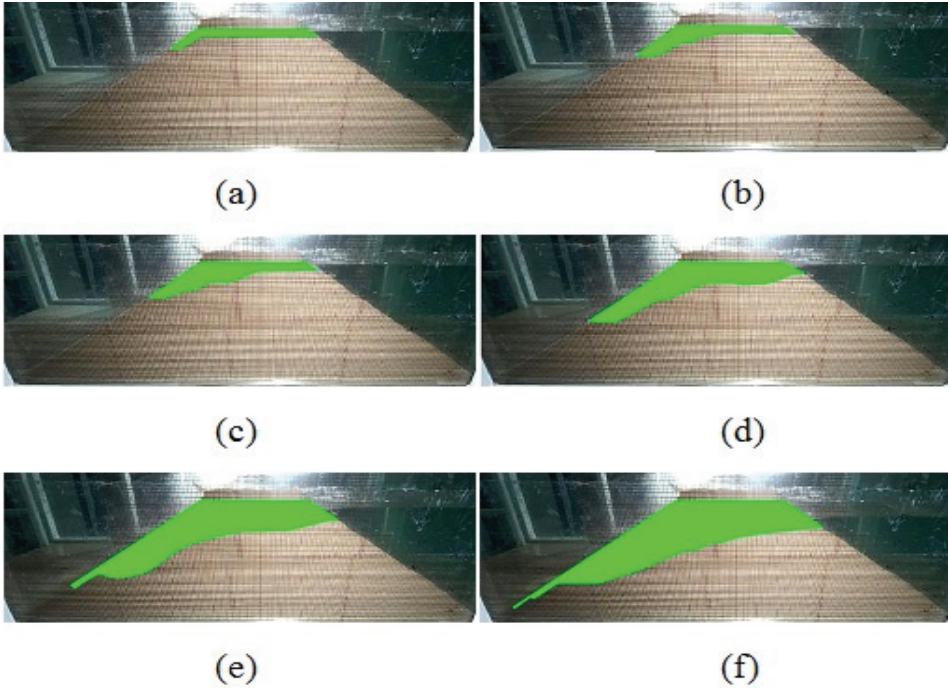
Figure 17 - The evaluation of eroded side area at different time instants a) t=10 sec, b) t=70 s, c) t=130 sec, d) t=190 sec, e) t= 250 sec, f) t=310 sec for case 2

The calculated breach area values were compared with those obtained from the Gauss Area method (Figs. 18 and 19).
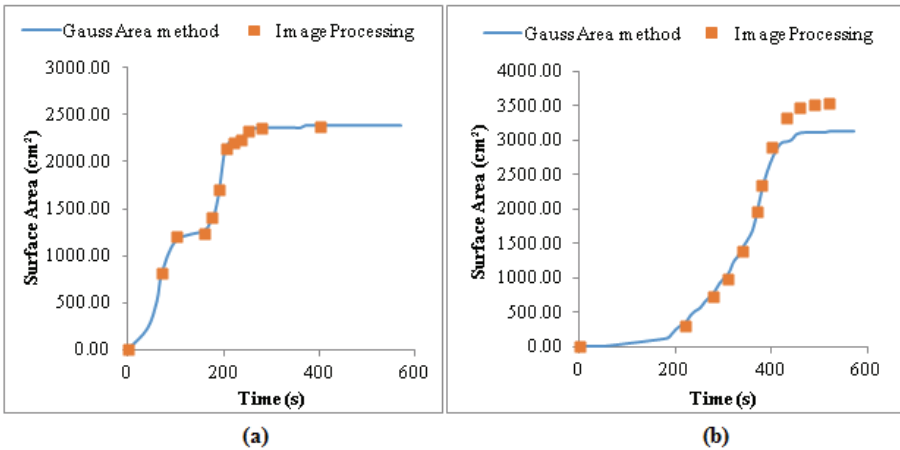

Figure 18 - Comparison of Gauss Area method and Image Processing results for case 1 a) at downstream b) at upstream
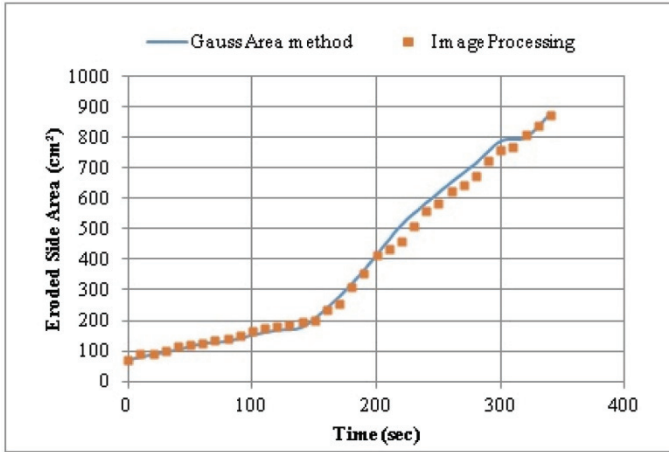
Figure 19 - Comparison of Gauss Area method and Image Processing results for the 2nd case

A very good agreement was found between the area values obtained from these two different approaches for both cases 1 and 2. Consequently, it was demonstrated that either of these approaches can be used to determine the time-dependent breach areas.

5. COMPARISON OF THE EXPERIMENTAL RESULTS BY DIMENSIONLESS CURVES

The dimensionless time-dependent curves were also generated to obtain the universal curves which can be used in the cases of homogeneous earth-fill dams having different dimensions and under various hydraulic conditions.

The dimensionless parameters are generated by dividing the time dependent values of the parameter in question to its maximum value. The time elapsed to reach the maximum flow rate Q_{max} is denoted by t_Q. Similar subscripts are used for the maximum value of other parameters. The obtained dimensionless time varied flow rates, breach areas and breach widths versus dimensionless time curves are given in Figs 20, 21, 22, 23 and 24, respectively.

It was revealed that the dimensionless flow rates versus dimensionless time could be considered as two segment lines with two different slopes and two different stages, the first slope being smaller. The first stage lasted much longer in the 1st scenario.

The dimensionless breach areas versus dimensionless time in the 2nd scenario could be approximated to two segment lines while in the 1st scenario the linear behavior appeared only in the first stage.

The tendency of the dimensionless curves at upstream were found to be very different in the 1st and 2nd scenarios. The evolution of the dimensionless breach areas was nearly exponential in the 1st scenario whereas the evolution can be considered as combination of the straight
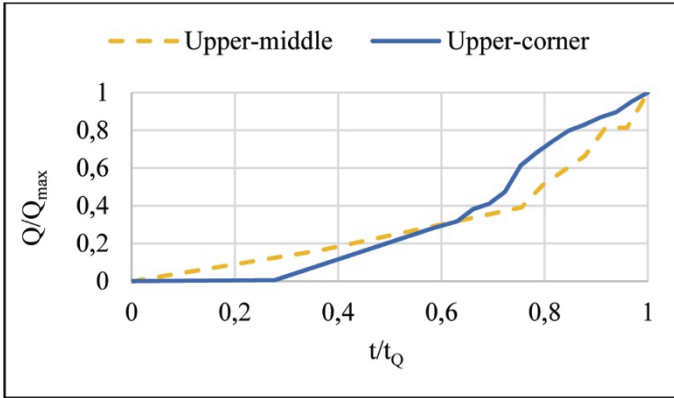
Figure 20 - Dimensionless flow rates versus dimensionless times curves
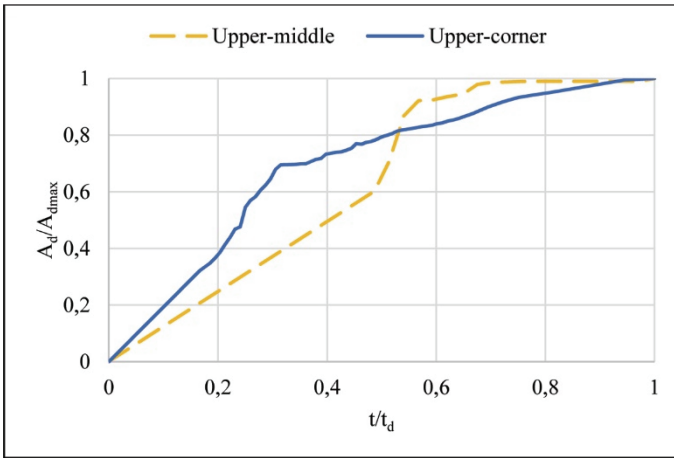

Figure 21 - Dimensionless breach areas at downstream versus dimensionless times curves
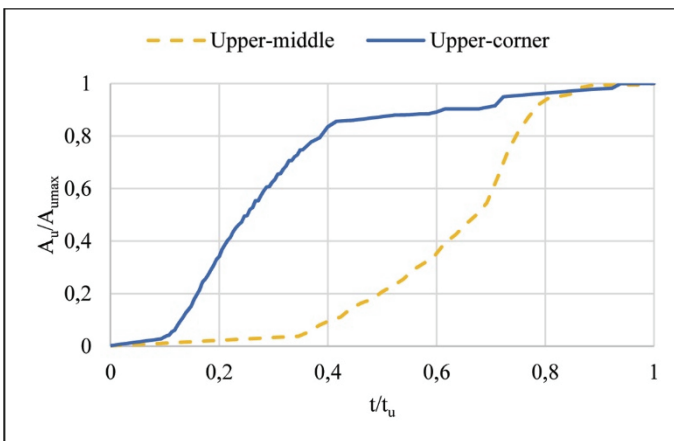

Figure 22 - Dimensionless breach areas at upstream versus dimensionless times curves

lines when the seepage initiated at corner. Besides, the upstream breach area was significant when t=0.4 t_u in the 2nd scenario while at this time the breach area was quite small and then increased significantly in the 1st scenario.

Figure 23 - Dimensionless breach widths at downstream versus dimensionless times curves

When t= 0.50 $t_{B,d}$ the breach width at downstream was almost B_d= 0.85 $B_{d,max}$ in the 2nd scenario, while B_d= 0.58 $B_{d,max}$ in the case of the 1st scenario.

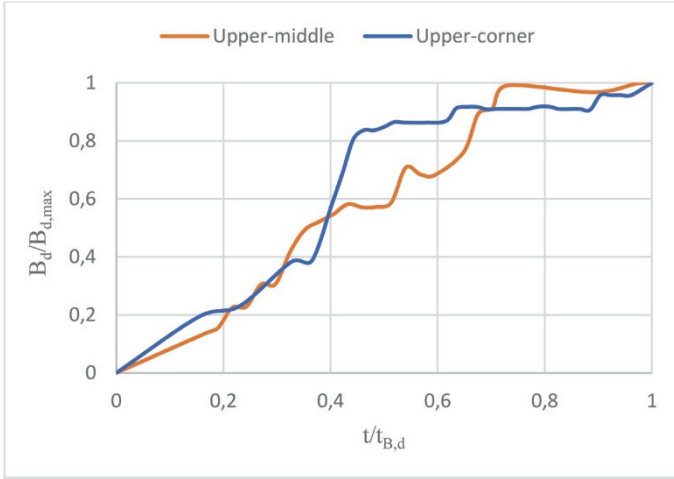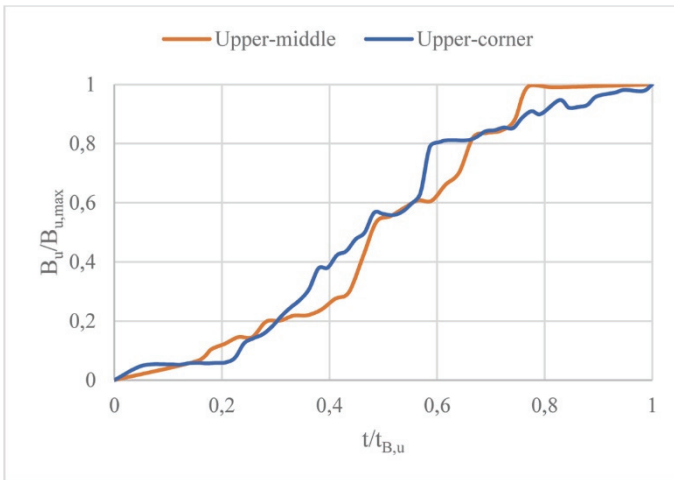*Figure 24 - Dimensionless breach widths at upstream versus dimensionless times curves*

When t= 0.50 $t_{B,u}$ the breach width at upstream was approximately B_u= 0.48 $B_{u,max}$ in both cases. In the 2nd scenario, the dimensionless breach width developed continuously but in the 1st scenario there was no change in dimensionless breach width beyond t= 0.76 $t_{B,u}$.

Nevertheless, the best compatibility was obtained in the case of the dimensionless upstream breach widths for both scenarios.

6. CONCLUSIONS

In this study, the failure of dam occurred mainly because of the head cut erosion. Head cut erosion directly started at the downstream surface of the dam where seepage initiated. While the water was seeping through the circular tunnel the material of the dam was moved away. Due to eroded material, piping enlarged causing the transportation of more material. Head cut erosion developed from downstream towards upstream. When breaching started, the orifice flow was converted to open channel flow where breach bottom behaved like a broad crested weir. At the same time, breach experienced widening until head cut reached the upstream surface. Afterwards, breach continued to enlarge longitudinally toward to channel bottom.

The breach areas obtained by using the Gauss area functions were found to be in accord with those obtained from the image processing method.

In the 2nd scenario, the lateral side being rigid influenced considerably the flow rate and the development of the breach. The peak flow rate corresponding to the 1st case was found to be approximately 2.3 times greater than that of 2nd case.

The maximum breach areas and average breach widths were found to be lower in the 2nd case due to the limited available space for the breach development. Consequently, the ratios between the values corresponding to the 1st and 2nd scenarios were found as 3.25 and 1.75 for maximum breach areas at downstream and at upstream sides, respectively. These ratios were 2.44 and 1.37 for the average breach widths at downstream and upstream sides, respectively.

This study revealed the temporal development of the breach mechanism in the cases where the seepage is located at the upper middle or upper corner of homogeneous earth-fill dam. In both cases the maximum breach areas and average breach widths at upstream side of the dam were found to be greater compared to those observed at downstream.

The dimensionless curves corresponding to time-dependent flow rates, breach areas and breach widths were also generated in order to get universal curves, making possible their use in the cases of other homogeneous earth-fill dams having different dimensions and under various hydraulic conditions, when the seepage starts at upper part of the dams.

These experimental findings provide the opportunities for the calibration and validation of the numerical models used in the relevant numerical investigations. This study also offers guidance for the strategies concerning emergency action plans related to the failure of homogeneous earth-fill dams when the seepage starts at upper part of the dams.

Since the piping phenomenon is a complicated phenomenon depending on several factors, it would be very useful to perform numerous experimental studies on the homogeneous earth-fill dams constructed with different mixtures, possessing different geometry with different piping locations. It would also be interesting to perform such experiments on earthen dams with clay core. A numerical model calibrated and validated according to such experimental findings would make possible the investigation of the behavior of the real dams in the case of piping.

Symbols

A_d	: temporal breach area at downstream
A_u	: temporal breach area at upstream
A_{umax}	: maximum breach area at upstream
$A_{d\,max}$	: maximum breach area at downstream
A_{latmax}	: maximum lateral breach area
B_d	: temporal breach width at downstream
B_u	: temporal breach width at upstream
C	: cohesion
C_c	: coefficient of gradation or compression index
CL	: low plasticity clay
C_s	: swell index
C_u	: coefficient of uniformity
C_{un}	: unconfined compression index
C_r	: recompression index
D	: grain diameter
E_{oed}	: Oedometric modulus of deformation
H_d	: dam height
I	: coordinate
i_{cr}	: critical hydraulic gradient
k	: coefficient of permeability
L	: dam length
LL	: Liquid Limit
n	: porosity
SC	: clayey sand
SG	: specific gravity
Q	: discharge from the breach
Q_{max}	: maximum flowrate from the breach
Q_{pump}	: flowrate delivered from the pump
x_i	: abscissa
y_i	: ordinate

w_{opt}	: optimum water content
ΔS	: storage in the channel
Δt	: time interval
γ_w	: unit weight of water
γ_{sat}	: saturated unit weight
$\gamma_{dry,max}$	: maximum dry unit weight
ϕ	: internal friction angle

Acknowledgements

References

[1] Zhong, Q., Wang, L., Chen, S., Chen, Z., Shan, Y., Zhang, Q., Ren, Q., Mei, S., Jiang, J., Hu, L., & Liu, J., Breaches of embankment and landslide dams - State of the art review. Earth-Science Reviews, 216, 103597, 2021. https://doi.org/10.1016/j.earscirev.2021.103597

[2] Robbins, B. A., & van Beek, V. M., Backward erosion piping: A historical review and discussion of influential factors. Association of State Dam Safety Officials, Dam Safety 2015, September, 2015.

[3] ASCE/EWRI Task Committee on Dam/Levee Breaching, Earthen Embankment Breaching. Journal of Hydraulic Engineering, 137, 12, 1549–1564, 2011. https://doi.org/10.1061/(ASCE)HY.1943-7900.0000498

[4] Sellmeijer, J. B. On the mechanism of piping under impervious structures [Bibliotheek Technische Universiteit], 1988. http://repository.tudelft.nl/assets/uuid:7f3c5919-1b37-4de9-a552-1f6e900eeaad/TR diss 1670(1).pdf

[5] Teton Dam History & Facts . http://www.usbr.gov/ssle/damsafety/index.html, 2016.

[6] Al-Janabi A.M.S., Ghazali A.H., Ghazaw Y.M., Afan H.A., Al-Ansari N., and Yaseen Z.M., Experimental and numerical analysis for earth-fill dam seepage. Sustainability, 12(6),2490, 2020. https://doi.org/10.3390/su12062490.

[7] Dhiman, S., and Patra, K. C., Experimental study of embankment breach based on its soil properties. ISH Journal of Hydraulic Engineering, Taylor & Francis, 26, 3, 247–257, 2020.

[8] Zhu, Y., Visser, P. J., Vrijling, J. K., and Wang, G., Experimental investigation on breaching of embankments. Science China Technological Sciences, 54, 1, 148–155, 2011.

[9]   Morris, M., Hassan, M., Kortenhaus, A., Geisenhainer, P., Visser, P., and Zhu, Y., Modelling breach initiation and growth. Flood Risk Management: Research and Practice, 581–591, 2008.

[10] Zomorodian, S. M. A., Noghab, M. J. A., Zolghadr, M., and O'Kelly, B. C., Overtopping erosion of model earthen dams analysed using digital image-processing method. Proceedings of the Institution of Civil Engineers: Water Management, 173, 6, 304–316, 2020.

[11] Sharif, Y. A., Elkholy, M., Hanif Chaudhry, M., and Imran, J., Experimental Study on the Piping Erosion Process in Earthen Embankments. Journal of Hydraulic Engineering, 141, 7, 04015012, 2015.

[12] Elkholy, M., Sharif, Y. A., Chaudhry, M. H., and Imran, J., Effect of soil composition on piping erosion of earthen levees. Journal of Hydraulic Research, 53, 4, 478–487, 2015.

[13] Annunziato, A., Santini, M., Proietti, C., Girolamo, L., Lorini, V., Gerhandinger, A., Tucci, M., Modelling and Validation of the Derna Dam Break Event GeoHazards, 5, 2, 504-529, 2024. https://doi.org/10.3390/geohazards5020026.

[14] Guney, M. S., Dumlu, E., Okan, M., and Tayfur, G., Experimental Study of Breach Evolution and Discharge Through Breach Resulting from Piping due to Seepage at the Upper Corner of in an Earth-Fill Dam. 14th International Conference on Hydroscience & Engineering (ICHE 2022) MAY 26-27, 2022, İzmir, Turkey, 99–109, 2022a.

[15] Guney, M. S., Okan, M., Dumlu, E., Bor, A., Aklık, P., and Tayfur, G., Experimental Study of the Evolution of the Breach and the Discharge Through the Breach Resulting from Piping due to Seepage at the Earth-Fill Dam Top. Proceedings of the 39th IAHR World Congress 19-24 June 2022, Granada, Spain, 2735–2743, 2022b.

[16] Ojha, C. S. P., Singh, V. P., and Adrian, D. D., Influence of Porosity on Piping Models of Levee Failure. Journal of Geotechnical and Geoenvironmental Engineering, 127, December, 1071–1074, 2001.

[17] Richards, K. S., and Reddy, K. R., Critical appraisal of piping phenomena in earth dams. Bulletin of Engineering Geology and the Environment, 66, 4, 381–402, 2007.

[18] Terzaghi, K., Peck, R. B., and Mesri, G., Soil mechanics in engineering practice. Wiley, New York, 1996.

[19] Okan, M., Experimental and Numerical Investigation of Piping in Uniform Embankment Dam with Weak Layer at the Upper Region. M.Sc. Thesis, İzmir Institute of Technology, 2022.